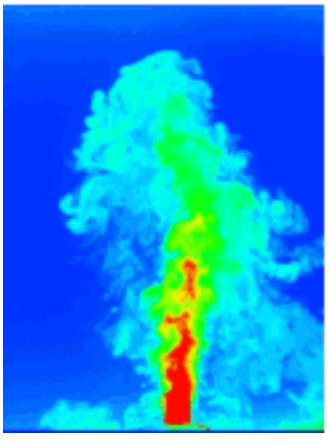

Journal of Turbulence
Publication details, including instructions for authors and subscription information:
http://www.tandfonline.com/loi/tjot20

LES modeling of converging-diverging turbulent channel flow

Lukasz Kuban [a], Jean-Philippe Laval [b c], Witold Elsner [a], Artur Tyliszczak [a] & Matthieu Marquillie [b c]

[a] Institute of Thermal Machinery, Czestochowa University of Technology, Czestochowa, Poland

[b] CNRS, UMR 8107, Villeneuve d'Ascq, France

[c] Université Lille Nord de France, Lille, France

Available online: 16 Mar 2012

To cite this article: Lukasz Kuban, Jean-Philippe Laval, Witold Elsner, Artur Tyliszczak & Matthieu Marquillie (2012): LES modeling of converging-diverging turbulent channel flow, Journal of Turbulence, 13, N11

To link to this article: http://dx.doi.org/10.1080/14685248.2012.661062

Journal of Turbulence
Vol. 13, No. 11, 2012, 1–19

LES modeling of converging-diverging turbulent channel flow

Lukasz Kuban[a], Jean-Philippe Laval[b], Witold Elsner[a]*, Artur Tyliszczak[a] and Matthieu Marquillie[b]

[a] *Institute of Thermal Machinery, Czestochowa University of Technology, Czestochowa, Poland*
[b] *CNRS, UMR 8107, Villeneuve d'Ascq, France, and Université Lille Nord de France, Lille, France*

(*Received 20 July 2011; final version received 18 January 2012*)

The paper presents the results of the application of large-eddy simulation (LES) to turbulent channel flow with a varying pressure gradient obtained by an appropriately specified shape of one of the walls. The main objective of the paper is to assess various subgrid scale (SGS) models implemented in two different codes as well as to assess the sensitivity of the predictive accuracy to grid resolution. Additionally, the role of SGS viscosity, controlled by a constant parameter of the SGS model, was investigated. The simulations were performed with inlet conditions corresponding to two Reynolds numbers: $Re_\tau = 395$ and $Re_\tau = 617$. The consistency and the accuracy of simulations are evaluated using direct numerical simulation (DNS) results. It is demonstrated that all SGS models require a comparable minimum grid refinement in order to capture accurately the recirculation region. Such a test case with a reversal flow, where the turbulence transport is dictated by the dynamics of the large-scale eddies, is well suited to demonstrate the predictive features of the LES technique.

Keywords:

1. Introduction

Large-eddy simulation (LES) is a technique that has become increasingly popular over the past 20 years. The concept behind LES is to directly solve large turbulent eddies that are proportional to a given mesh and to model the influence of nonresolved scales onto resolved ones. The LES technique is increasingly used as a tool to model such problems as nonequilibrium, three-dimensional flows, relaminarizing, retransitioning boundary layers, and massively separated flows. The main limitation of LES appears to be in its application for wall-bounded flow. In this case, when the near-wall region needs to be resolved, the grid must be proportional to the size of the small inner-layer eddies, which is strongly dependent on the Reynolds number. It is known that these small structures have a major impact on the entire flow and the LES approach has to capture an essential part of their dynamics. This forces the necessary mesh density, especially in the wall-normal direction, and thus raises the computational cost. On the other hand, the quality of the solution of the near-wall flow depends, among other things, on the applied subgrid scale (SGS) model.

The accuracy of the LES solution depends strongly on two main sources of errors, introduced, on one hand, by the discretization method and, on the other hand, by the SGS model. The more so, as it was presented by Meyers et al. [1, 2] those two errors interact

*Corresponding author. Email: welsner@imc.pcz.czest.pl

ISSN: 1468-5248 online only

http://dx.doi.org/10.1080/14685248.2012.661062
http://www.tandfonline.com

strongly one with the other. Eddy viscosity SGS models, applied for wall-bounded flows, should possess suitable properties. They should produce an eddy viscosity with correct near-wall behavior and need to model properly the energy transfer from the resolved scales to the subgrid ones through the SGS dissipation. The discretization error, which influences the level of SGS dissipation, depends not only on the chosen discretization method but also on the numerical implementation of the model.

The importance of these sources of errors has received wide attention in the literature in the past years. Already, Piomelli and Balaras [3] have emphasized that a typical outer-layer discrepancy in the velocity profile observed in LES of adverse pressure gradient flows might be due to SGS errors. The review of LES assessment for both homogeneous isotropic turbulence and boundary-layer flows has been given by Meyers [4]. His analysis drew attention to the need of proper selection of Smagorinsky coefficient and near-wall damping in order to obtain good logarithmic velocity profiles and turbulence spectra. For the testing and development of SGS models, plane channel flow is often taken as a first choice. Fröhlich et al. [5] investigated LES channel flow for two Reynolds numbers, i.e., 180 and 395, with three SGS models: Smagorinsky, dynamic Smagorinsky, and dynamic mixed model. They have shown that the best match with direct numerical simulation (DNS) data for the lower Reynolds number was obtained with dynamic Smagorinsky model, while for the higher Reynolds number, with dynamic mixed model. The paper also suggests that numerical discretization has a non-negligible impact on the computed fluctuations. However, Meyers and Sagaut [6], studying the grid convergence behavior of channel-flow DNS, emphasized that a caution is needed when evaluating SGS models. They claim that very often, the conclusion, that a given SGS model performs better than the other, is a coarse-resolution-related artifact. The greater difficulties arise for such a group of wall-bounded flows when the turbulent boundary layer separates from the curved wall due to a geometry-induced adverse pressure gradient. In such cases, the structure of the upstream flow influences the separation and, even more strongly, the reattachment point. Large-scale structures also play a dominant role within the separated shear layer as well as in the recirculation zone, which should be well resolved using the LES technique. The test case often used for the analysis of separated flow is a channel with a periodic arrangement of hills [7, 8, 9]. Fröhlich et al. [7] state that the simulation of separation from curved surfaces can be very sensitive to the grid density and the details of the near-wall treatment as well as the nature of the SGS model. They proved that the sensitivity appears to be rooted mainly in variations of the predicted separation point. Hahn and Drikakis [8] raised the problem of discretization claiming that the higher order methods yield an improvement in predicting the averaged separation point even if the boundary layer is underresolved, although they confirmed that it is almost impossible to isolate the effects of the numerical method on individual regions. They stated, however, that compared to low-order schemes, applying the high-order discretization method allows the accuracy of the solution to be maintained while reducing the number of mesh points. The most popular methods that are characterized by smaller numerical error are spectral and compact difference methods. Although the use of these methods is very limited in complex geometries, their applications in simple domains with a structured code allows the role of the SGS model in basic flows to be analyzed.

The aim of the paper is to asses the discretization methods and various SGS models implemented in two different codes, one, MFLOPS3D, developed at Laboratoire de Mecanique de Lille (LML hereinafter) and the other SAILOR developed at Czestochowa University of Technology (CUT hereinafter). This problem has already been discussed, to a limited extent, by Laval et al. [10]. In that study, the inlet conditions were generated separately by LML and CUT, which might have induced a slight discrepancy in the statistics in

the adverse pressure gradient region. In the present work, the same inflow as for the reference DNS calculation is used for simulations with both codes. Additionally, more detailed analyses of the SGS models and mesh refinement effects on the results are investigated. The reference case is a turbulent channel flow with inlet conditions corresponding to the Reynolds numbers $Re_\tau = 395$ and $Re_\tau = 617$ at the inlet (based on friction velocity u_τ and half channel height h) with a varying pressure gradient calculated with DNS by Marquillie et al. [11]. The shape of the channel is characterized by the same cross-section at both the inlet and outlet. A bump is located on the lower wall producing a favorable pressure gradient (FPG), followed by an adverse pressure gradient (APG). The strong APG downstream of the summit of the bump leads to a small separation of the flow at the lower curved wall. The models considered in the paper are the classical Smagorinsky with damping function (SM), the Shear-Improved Smagorinsky (SISM) [12], the Dynamic Smagorinsky (DSM), and the Wall-Adapting Local Eddy-Viscosity (WALE) model of Nicoud and Ducros [13]. The adopted test cases could be regarded as useful engineering test cases because they allow the predictive features of LES for the simulation of APG flow with and without a small separation to be demonstrated.

2. Numerical code

Both SAILOR and MFLOPS3D have been developed based on similar assumptions even though the initial scope of these two codes is different. The SAILOR code is based on the projection method [14] for the pressure–velocity coupling. The time integration is performed by the 2nd order predictor–corrector Adams–Bashforth/Adams–Multon scheme. The spatial derivatives are approximated by Fourier approximation in the spanwise direction and a high-order compact scheme [15] in the wall normal and streamwise direction.

The high-order discretization (6th order for the inner nodes) allows for a coarsening of the grid and at the same time preserving accurate results. MFLOPS3D also relies on the projection method for the pressure–velocity coupling. Spectral spanwise and normal discretization combines the advantage of good accuracy with a fast integration procedure when compared to a standard numerical procedure for complex geometries. MFLOPS3D uses Fourier discretization in spanwise directions, Chebyshev Collocation in the normal direction, and a 2nd-order backward Euler differencing for time integration. In MFLOPS3D, the Chebyshev collocation in the wall-normal y-direction can lead to aliasing errors. Aliasing is usually not critical for DNS because the level of kinetic energy is very low for the smallest resolved modes since the discretization must be sufficient to resolve all turbulent scales. In LES, and especially coarse LES, the kinetic energy at the smallest resolved modes is significant and leads to aliasing errors. In order to overcome this effect, an explicit filtering was used in the normal direction only. The explicit filter must be smooth enough to remove the aliasing effect but sharp enough to keep a sufficient spectral resolution in this direction. In MFLOPS3D, it was decided to chose a raised cosine filter. This filter was used by Pasquetti et al. in order to weaken the Gibbs phenomenon of the pseudo-penalization method [16]. In 1D, the raised cosine filter is defined in the spectral space by:

$$\hat{g}(k) = \frac{1}{2}\left(1 - \cos(2\pi k/N)\right); |k| < N/2, \tag{1}$$

where k is the Fourier mode. No explicit filtering was used in the spanwise and streamwise direction.

In both codes, there is a homogeneous distribution of nodes in the spanwise and streamwise direction. However, different discretization schemes for both codes were applied in streamwise direction. CUT code uses compact discretization scheme, whereas the LML code uses a 4th-order finite differences scheme. Furthermore, the application of different discretization schemes in the normal direction causes, even when the total number of grid points is the same, different grid spatial resolutions in the wall vicinity, and this problem is addressed in the next section. Both codes are structured grid solvers, where instead of writing the Navier–Stokes system in curvilinear coordinates, the wall curvature was obtained by a mathematical mapping of the partial differential operators from physical coordinates to Cartesian ones. More details about MFLOPS3D and the mapping of coordinates can be found in [11].

3. Subgrid-scale models

It is well known that in wall-bounded flows, it is crucial to describe the behavior of the small turbulent structures created near the wall properly. This means that SGS models have not only to model properly the energy transfer from the resolved scales to the subgrid ones, but also to present correctly the eddy viscosity distribution in the wall-normal direction. In the paper results, samples obtained with the classical Smagorinsky, dynamic Smagorinsky (DSM), and the WALE models are presented, where the classical Smagorinsky and WALE were applied in the SAILOR code and DSM and WALE in the MFLOPS3D code. Because the eddy viscosity in the classical Smagorinsky model is not properly scaled near the wall, a damping function $\mathcal{D}$, similar to the van Driest damping formula, was used. The function was defined as:

$$\mathcal{D} = \left(1 - \exp\left(\frac{-|y^+|}{26}\right)\right)^3.$$

The Lilly formulation [17] of the dynamic Smagorinsky model with a sharp spectral cutoff test filter in the spanwise direction (keeping half Fourier modes) was used. An explicit five-point filter with three vanishing moments is used in physical space for the streamwise direction: $\widetilde{u}_i = -u_{i-2}/16 + u_{i-1}/4 + 5u_i/8 + u_{i+1}/4 - u_{i+2}/16$. The test filter width was estimated as $\sqrt[3]{4}\ \Delta$, where, for both solvers, the characteristic filter width Δ is defined as $\Delta = \sqrt[3]{\Delta_x \Delta_y \Delta_z}$. To stabilize the solution, the results of the estimated dynamic Smagorinsky constant C_s by the dynamic procedure were averaged in the homogeneous spanwise direction.

An interesting alternative to the Smagorinsky model is the WALE model [13], which is based on the square of the velocity gradient tensor and accounts for the effects of both the strain and the rotation rate to obtain the local eddy viscosity. As it is based, by definition, on local quantities, the model is suitable for the simulation of complex geometries. Additionally, it recovers the proper near-wall scaling for the eddy viscosity without requiring a dynamic procedure.

Another way to adapt the Smagorinsky model to the near-wall region is to use the shear-improved Smagorinsky model (SISM) [12]. In this improved version, the Smagorinsky eddy-viscosity is modified as $\nu_t = (C_s\Delta)^2(|\overline{S}| - |\langle\overline{S}\rangle|)$: the magnitude of the mean shear $|\langle\overline{S}\rangle|$ is subtracted from the magnitude of the instantaneous resolved rate-of-strain tensor $|\overline{S}|$ and C_s is the standard Smagorinsky constant. The angle brackets denote principally, an ensemble average, which, in practice, in our case, is a space average over the spanwise homogeneous direction.

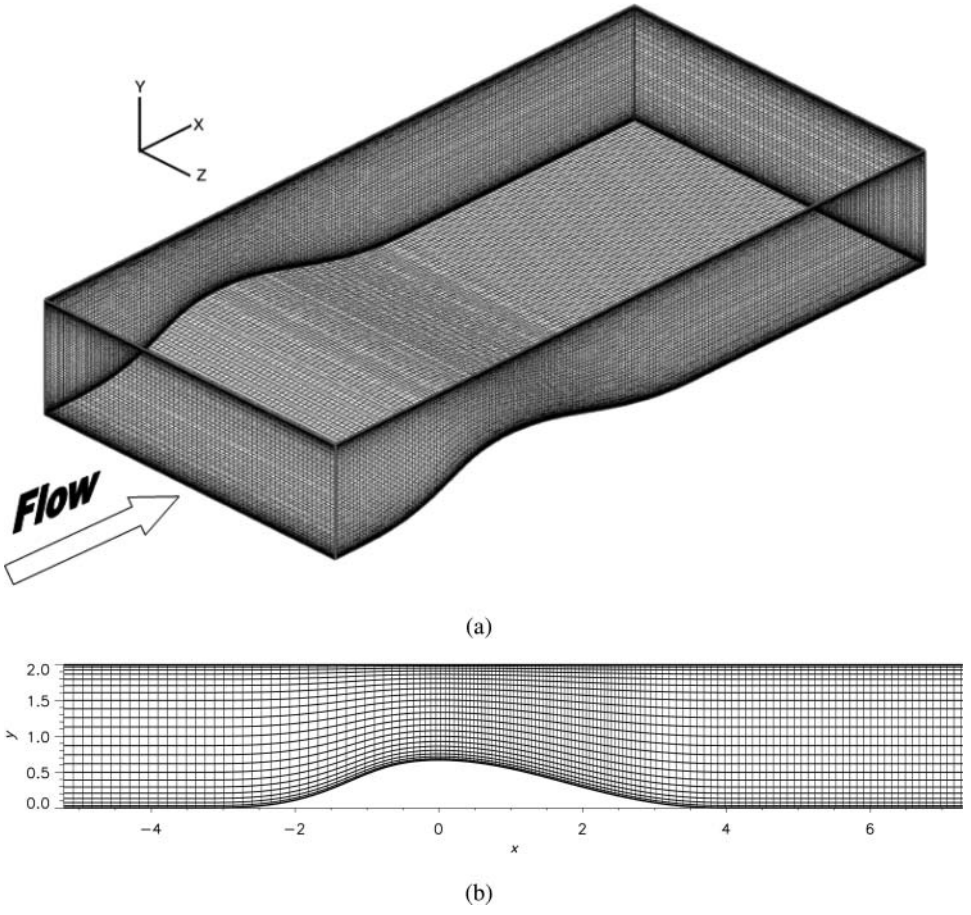

Figure 1. The computational domain: general view (a) and the mesh with stretching for $Re_\tau = 617$ (every 16 meshes in each direction) (b).

4. Test case description

The computational domain corresponds to the one used in experiments conducted in the wind tunnel at the Laboratorie de M canique de Lille at a high Reynolds number. Marquillie et al. [11, 18] performed DNS of this test case for the Reynolds number $Re_\tau = 395$ and $Re_\tau = 617$. The spatial resolution for the two DNS are $1536 \times 257 \times 384$ and $2304 \times 384 \times 576$, respectively. These two DNS are used as a benchmark for the validation of the set of LES.

A general view of the computational domain is presented in Figure 1. The CUT domain is 4π long, 2π wide in the spanwise direction based on half the channel height at the inlet, whereas the domain used by LML is only π wide in the spanwise direction. Two types of mesh repartition are used in the streamwise direction. For $Re_\tau = 395$, the mesh is uniform, while for $Re_\tau = 617$ the mesh is densified downstream the summit of the bump (see Figure 1).

The results of LES with four SGS models are compared with several grid refinements. The simulation parameters, as well as spatial resolutions of each LES, are given in

Table 1. Parameters of the DNS and LES calculations. The space discretizations in wall units (Δx^+, Δy^+, Δz^+) are the maximum values in each direction computed with the friction velocity at the summit of the bump. C is the constant of the subgrid-scale model. N_z is the number of grid points in the spanwise size of π even if the simulation with SAILOR code were performed on a domain twice as large.

Name	Model	Code	Re_τ	N_x	N_y	N_z	Δx^+	Δz^+	$\Delta y^+_{\min}$	$\Delta y^+_{\max}$	C
D00	DNS	MFLOPS3D	395	1536	257	384	5.1	5.1	0.03	5.1	—
D01	DNS	MFLOPS3D	617	2304	384	576	5.7	3.8	0.01	3.8	—
M01	WALE	MFLOPS3D	395	384	129	96	20.4	20.3	0.12	10.2	0.4
M02	WALE	MFLOPS3D	395	256	129	48	30.6	40.7	0.12	10.3	0.4
M03	WALE	MFLOPS3D	395	256	65	48	30.6	40.7	0.50	20.3	0.4
M04	WALE	MFLOPS3D	395	256	65	48	30.6	40.7	0.50	20.3	0.2
M05	DSM	MFLOPS3D	395	256	65	48	30.6	40.7	0.50	20.3	—
M06	NONE	MFLOPS3D	395	256	65	48	30.6	40.7	0.50	20.3	—
M07	WALE	MFLOPS3D	395	256	65	24	30.6	81.4	0.50	20.3	0.4
M08	WALE	MFLOPS3D	395	192	65	48	40.9	40.7	0.50.	20.3	0.4
M09	WALE	MFLOPS3D	395	96	65	24	81.8	81.4	0.50.	20.3.	0.4
M10	NONE	MFLOPS3D	395	96	65	24	81.8	81.4	0.50	20.3	—
S01	NONE	SAILOR	395	192	96	32	40.9	61.0	1.0	19.6	0.0
S02	WALE	SAILOR	395	192	96	32	40.9	61.0	1.0	19.6	0.2
S03	WALE	SAILOR	395	192	96	32	40.9	61.0	1.0	19.6	0.4
S04	SM	SAILOR	395	192	96	32	40.9	61.0	1.0	19.6	0.1
S05	NONE	SAILOR	395	96	96	32	81.8	61.0	1.0	19.6	0.0
S06	WALE	SAILOR	395	96	96	32	81.8	61.0	1.0	19.6	0.2
S07	WALE	SAILOR	395	96	96	32	81.8	61.0	1.0	19.6	0.4
S08	SM	SAILOR	395	96	96	32	81.8	61.0	1.0	19.6	0.1
M11	WALE	MFLOPS3D	617	576	193	144	22.8	15.1	0.06	7.6	0.4
M12	WALE	MFLOPS3D	617	288	97	72	45.6	30.2	0.25	15.1	0.4
M13	WALE	MFLOPS3D	617	288	97	72	45.6	30.2	0.25	15.1	0.3
M14	WALE	MFLOPS3D	617	288	97	72	45.6	30.2	0.25	15.1	0.6
M15	DSM	MFLOPS3D	617	288	97	72	45.6	30.2	0.25	15.1	—
M16	SISM	MFLOPS3D	617	288	97	72	45.6	30.2	0.25	15.1	0.09
M17	NONE	MFLOPS3D	617	288	97	72	45.6	30.2	0.25	15.1	—
M18	WALE	MFLOPS3D	617	288	65	48	45.6	45.4	0.55	22.6	0.4
M19	WALE	MFLOPS3D	617	192	65	48	68.4	45.4	0.55	22.6	0.4

Table 1. N_x, N_y, and N_z are the number of grid points in the streamwise, normal, and spanwise direction, respectively, while the given space discretization in wall units (Δx^+, Δy^+, Δz^+) corresponds to the maximum values computed with the friction velocity at the summit of the bump. A wall-resolved LES has to capture the effects of small turbulent structures originating near the wall, which affect the entire flow, so it is clear that the near-wall solution depends strongly on the grid quality. In the following work, the mesh spacing varies in the streamwise direction from $\Delta x^+ \simeq 20$–80, in the wall-normal direction from $\Delta y^+ \simeq 0.1$–20, and in the spanwise direction from $\Delta z^+ \simeq 15$–80. In this paper, the main focus of attention is on the region downstream of the minimum pressure point. The results presented by Laval et al. [10] have shown that an increase in resolution in the spanwise and normal direction does not lead to significantly better results at the lower wall, although it does better reproduce the boundary layer behavior on the upper flat plate.

For the simulations with MFLOPS3D, the normal resolution corresponds to the number of Chebyshev modes (before the filtering process of Equation (1), whereas for the SAILOR solver, a simple one-parameter hyperbolic tangent stretching function was used. The three

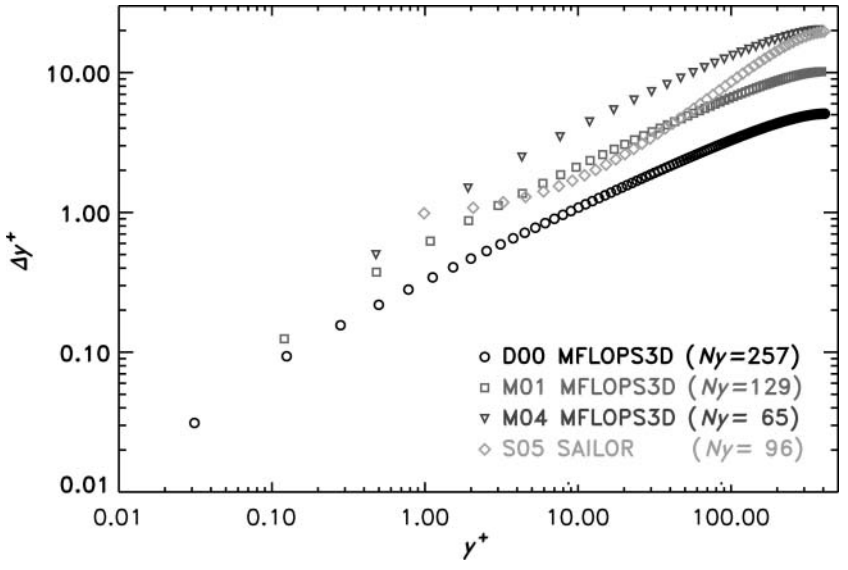

Figure 2. Comparison of the normal spatial resolution at the summit of the bump of the three LES grids and the DNS grid. The distances are normalized with the DNS friction velocity at the summit of the bump.

normal resolutions used for $Re_\tau = 395$ are compared to the DNS in Figure 2. It is clear that the normal resolution used by the SAILOR code with $N_y = 96$ is comparable to the normal resolution used by MFLOPS3D in most of the viscous sublayer and in the buffer layer ($2 < y^+ < 60$) with $N_y = 129$ and closer to the resolution of 65 in the outer layer. The time step is kept constant ($\Delta t = 10^{-3}$) for all the LES with MFLOPS3D in order to avoid any possible effect on the results and to maintain focus solely on the model effect. Whereas for SAILOR, the time step is dynamically computed based on CFL number equal to 0.8, i.e., the code searches for the maximum velocity in the flow field and then knowing the minimum mesh size the time step is computed. The inlet flow field at $Re_\tau = 395$ in both solvers was generated exactly for each time step in the same manner from a precursor well-resolved LES of flat channel flow. For the other test case ($Re_\tau = 617$), the inlet flow field was taken from precursor DNS calculations.

Whereas for SAILOR, the time step is dynamically computed based on CFL number equal to 0.8, i.e., the code searches for the maximum velocity in the flow field and then knowing the minimum mesh size the time step is computed.

5. Results

The first parameter characterizing the test case is the pressure coefficient defined as $Cp = \frac{\tau_w}{0.5\rho U_0^2}$, where U_0 is the maximum velocity at the inlet. The distribution of Cp for the upper and lower wall, obtained by the two solvers and the WALE model, and compared to DNS data ($Re_\tau = 395$) are presented in Figure 3. It can be seen that the pressure gradient is much stronger for the lower curved wall than for the flat wall. On the upper flat wall, the pressure gradient is too weak to induce separation, while on the lower wall, one can observe a typical diffusion zone indicating reversed flow between $x = 0.7$ and 1.5. The LES results overlap with the DNS data, which means that the simulation captures the main

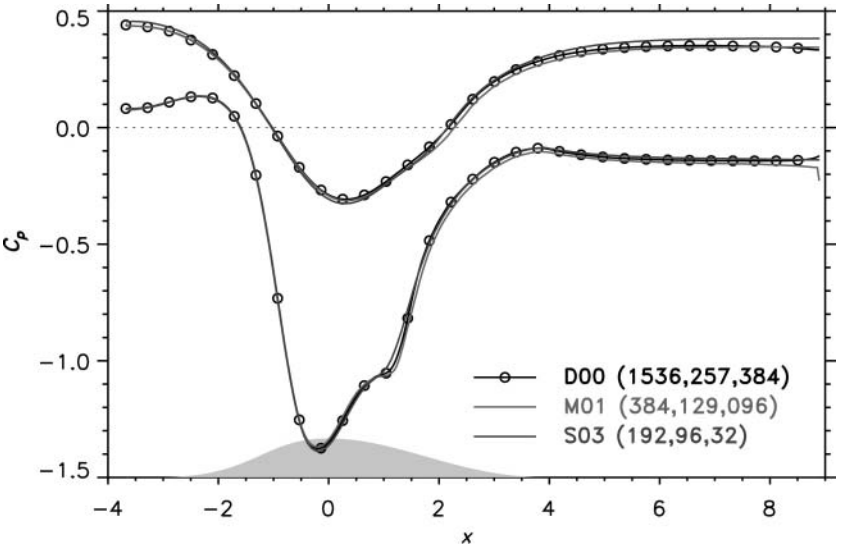

Figure 3. Pressure coefficient distribution for $Re_\tau = 395$ obtained with WALE model applied to both solvers.

flow behavior well. When simply analyzing the quality of the LES solutions, all possible errors are mixed together and are impossible to separate. A very detailed analysis of this type of interactions is presented in [9,10] where the authors managed to find the optimum of the Smagorinksky constant for assumed multiparametric criterion. These studies were related to the filter width, numerical scheme, and the numerical mesh. We believe that a similar procedure could be formulated also in our case. The difficulties are related to a general definition of the multiparametric criterion when looking for an optimum of the model constant. This seems to be problem specific and certainly could not be generalized for all other cases. We note that applying the high-order disrectization, the numerical errors are small and therefore one could expect that the interactions with the modeling errors are negligible; nevertheless, they cannot be completely excluded. However, it seems that the influence of the mesh density and location of the cutoff frequency related to the filter width is more important. For instance, increasing the mesh density leads to a reduction in the characteristic grid spacing and shifts the cutoff wavenumber toward the smaller scales. This causes overestimation of SGS viscosity ν_t and excessive dumping of turbulent kinetic energy within the flow. This fact is particularly important for the lower Reynolds number, where the cutoff filter could be located at the beginning of the dissipation range and not within the inertial range. Bearing in mind the above statements, the influence of grid density on the solution for $Re_\tau = 395$ is first considered.

To assess the role of the grid quality, it was initially decided to rely on the skin friction coefficient, defined as $C_f = \frac{\tau_w}{0.5\rho U_0^2}$,, which is one of the most important parameters of the boundary layer. Figure 4a and Figure 4b shows a comparison of the skin friction coefficient distributions for the upper flat and lower curved wall for various mesh refinements. All the results were obtained using the WALE SGS model with a constant $C_w = 0.4$ and MFLOPS3D solver. The main conclusion which can be drawn from this comparison is that the resolution in the spanwise direction within the range $N_z = 24$–48 ($\Delta z^+ = 81.4$ and 40.7) has a rather negligible effect on the solution (case M03 versus M07). Looking more

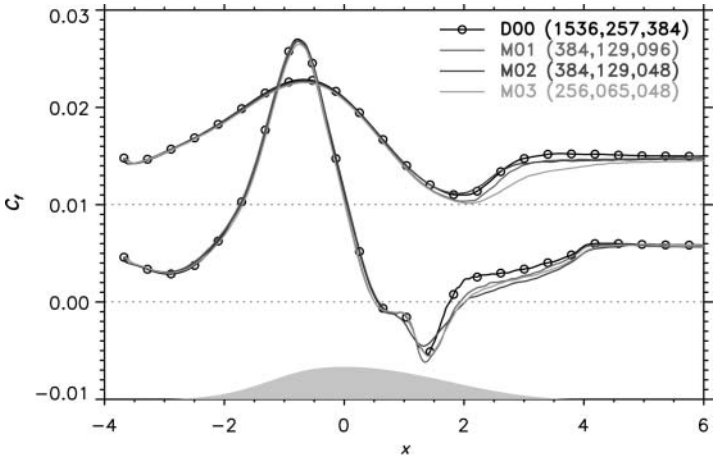

(a) MFLOPS3D, WALE model, $Re_\tau = 395$

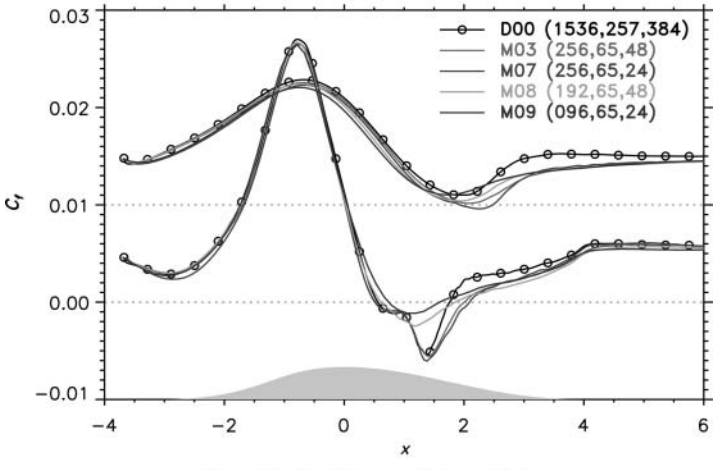

(b) MFLOPS3D, WALE model, $Re_\tau = 395$

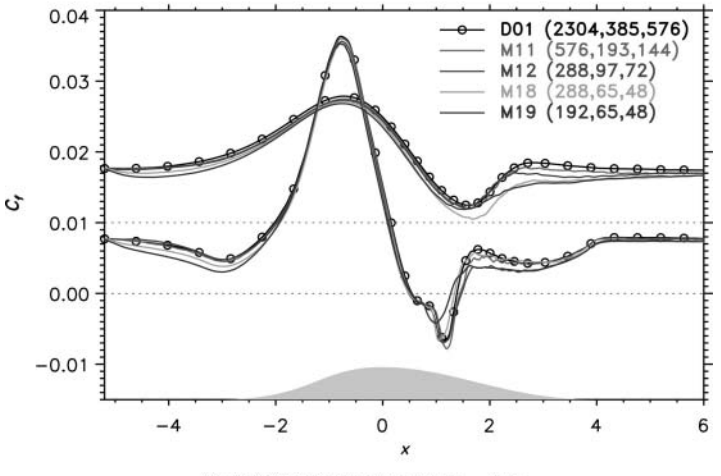

(c) MFLOPS3D, WALE model, $Re_\tau = 617$

Figure 4. Skin friction coefficient for different grid sizes using MFLOPS3D and the WALE subgrid-scale model for two different Reynolds numbers: $Re_\tau = 395$ ((a) and (b)) and $Re_\tau = 617$ (c).

closely at the results, one can notice that a very coarse spanwise resolution ($N_z = 24$) leads to acceptable results at the lower wall but does predict a slight unphysical separation at the upper wall. Therefore, it can be said that the number of grid points used by CUT, i.e., $N_z = 32$ could be acceptable for the comparison. One can also observe that the refinement from 65 to 129 in normal direction only slightly alters the results at the lower wall near the separation region but significantly improves the results at the upper wall (Figure 4a, cases M02 vs. M03). When analyzing the effect of the streamwise discretization, it seems that a minimum resolution of 256 corresponding to 30 wall units is required to correctly reproduce the separation region at the lower wall and that the two cases with the lowest streamwise resolution (M08 and M09) clearly underpredict the recirculation region. The same grid sensitivity study was performed for the highest Reynolds number (Figure 4c) and one can draw similar conclusions. A streamwise resolution of 45 wall units is sufficient to model the recirculation region at the lower wall (case M18). At the upper wall, however, the solution can be improved with a higher normal and spanwise resolution. In conclusion, it must be said that in contrast to the other two directions, the sensitivity of the solution of grid refinement in the streamwise direction was noticed. The results show that an increase in resolution in the spanwise and normal directions does not lead to significantly better results at the lower wall, although it does slightly better reproduce the boundary layer behavior on the upper flat plate. That is why any further considerations for $Re_\tau = 395$ will apply to the role of grid refinement in the streamwise direction only keeping $N_y = 65$ and $N_z = 48$ for LML and $N_y = 96$ and $N_z = 32$ for CUT calculations.

5.1. *Assessment of the role of the model constant*

In the next step, the effect of the grid refinement combined with simultaneous variation in the SGS model and the SGS viscosity is investigated. This is achieved by changing the value of the WALE model constant C_w . In Figure 5, skin friction coefficients are given for $Re_\tau = 395$ for $N_x = 96$ (coarse mesh – SAILOR results), $N_x = 192$ (fine mesh – SAILOR results), and $N_x = 256$ (super fine mesh – MFLOPS3D results), respectively. Each set of curves contains results for $C_w = 0.2$ and $C_w = 0.4$. The results are compared with the results obtained in equivalent cases not using the model but using the same explicit filtering. This means that in the third case, the SGS kinetic energy is not dissipated by the SGS model but that the explicit filtering participates in the overall dissipation. For a coarse mesh, the role of the SGS model is not seen explicitly in the zero and favorable pressure gradient region, but it is apparent in the APG region. For the case not using the model, the skin friction coefficients at both the upper and the lower wall are strongly overpredicted. At the lower wall, the separation is very small and the minimum of C_f, indicating the center of the recirculation zone, does not match DNS at all. This may suggest that the amount of kinetic energy generated and resolved in the APG gradient region is large and, therefore, a visible lack of dissipation by the SGS model is observed. Introducing an SGS viscosity through the SGS model with $C_w = 0.2$, improves the C_f. The most significant improvement is observed for $C_w = 0.4$. However, none of the cases considered are able to reproduce the correct C_f levels in the recirculation zone. The same effect of the model constant is observed for the upper and the lower wall. Assuming that the discrepancy in the results in the APG region is due to a too coarse mesh in the streamwise direction, the same models defined with the same constants are applied for a refined mesh ($N_x = 192$). By doubling the number of grid points from $N_x = 96$ to $N_x = 192$, the mesh spacing decreases from $\Delta x^+ \simeq 80$ to $\Delta x^+ \simeq 40$, shifting the smallest resolved scales in the dissipative range. The new set of C_f distributions is presented in Figure 5b. As expected, for the case without

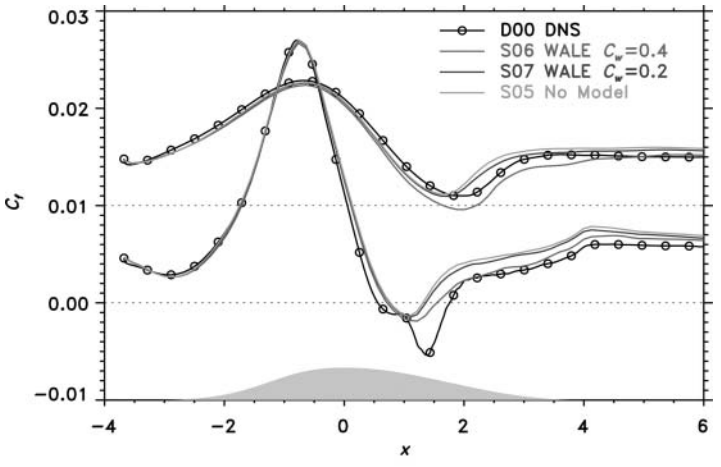

(a) SAILOR, WALE model, coarse mesh

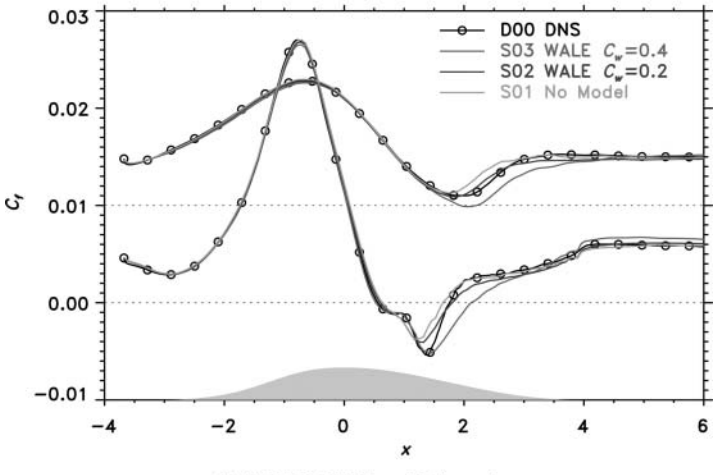

(b) SAILOR, WALE model, fine mesh

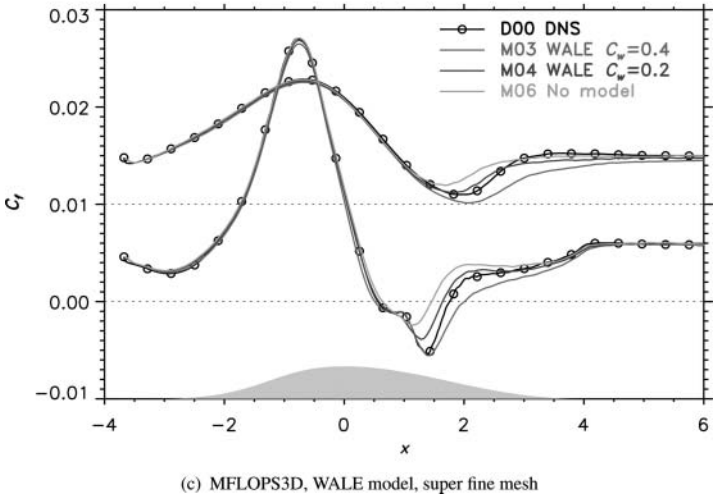

(c) MFLOPS3D, WALE model, super fine mesh

Figure 5. C_f distributions for WALE subgrid-scale model obtained for various mesh resolutions and the two numerical codes.

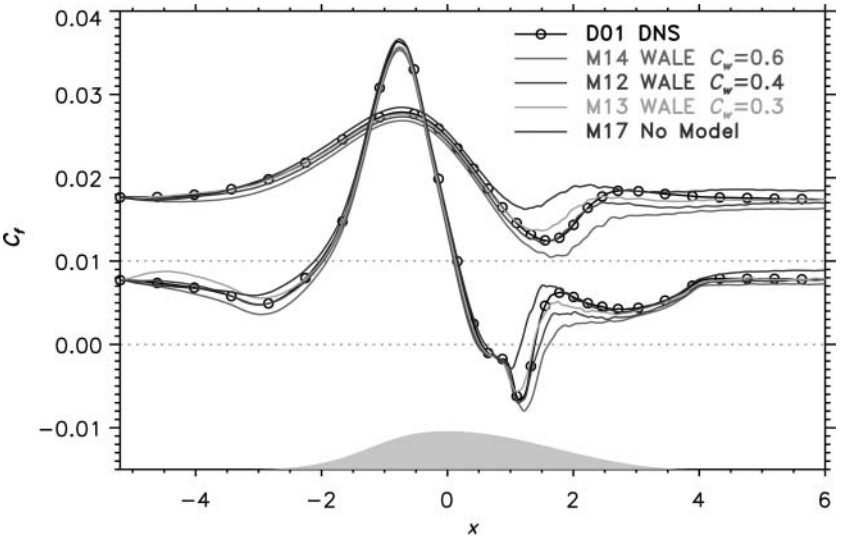

Figure 6. C_f distribution for the $Re_\tau = 617$ test cases with MFLOPS3D code.

the SGS model, an improvement is observed in comparison to the similar case on the coarse mesh. Increasing the model constant to 0.2 leads to a slightly better prediction for the C_f minimum and a shift of the C_f curve toward the DNS results. Surprisingly, for the case where the constant is equal to 0.4, clear overprediction of the reattachment point on the lower wall is noticed. The same tendency is observed for the upper wall, where the results obtained for a model constant equal to 0.2 are in much better agreement than those for 0.4. This observation leads to the conclusion that the mesh is fine enough and that the contribution of SGS viscosity (for WALE with $C_w = 0.4$) is already exaggerated. The final set of curves are for the super fine mesh ($N_x = 256$), obtained with the MFLOPS3D solver. For the case without the model, the skin friction is overestimated at both the upper and lower wall, while with $Cw = 0.4$, C_f is underestimated downstream of its minimum. The results show the interrelation between the grid density and SGS model constant for the constant $C_w = 0.4$ is not fully appropriate for our most refined case. Our study confirms that performing wall-resolved LES calculations without initial calibration of the SGS model constant is hazardous.

Figure 6 presents the effect of the model constant for the highest Reynolds test case. Despite the mesh refinement downstream of the summit of the bump, the case without the model does not allow us to capture the flow behavior properly as the C_f both close to the upper and lower wall is clearly overestimated. At the same time, it is clear that for $C_w = 0.6$, the SGS model introduces too much SGS dissipation, which results in underestimation of the C_f value at both the upper and lower walls, as well as overprediction of the position of the reattachment point. It is clear that the optimal model constant is not universal as it already differs for two cases at a similar low-Reynolds number.

Summarizing all the results presented in this section, one can state that similar behavior is observed for the three tested grids and for the two Reynolds number cases. In the range of tested resolutions, the best constant for the given geometrical configuration and the WALE model can be estimated as between 0.2 and 0.4. However, none of the tested constants for the particular cases leads to excellent near-wall agreement throughout the

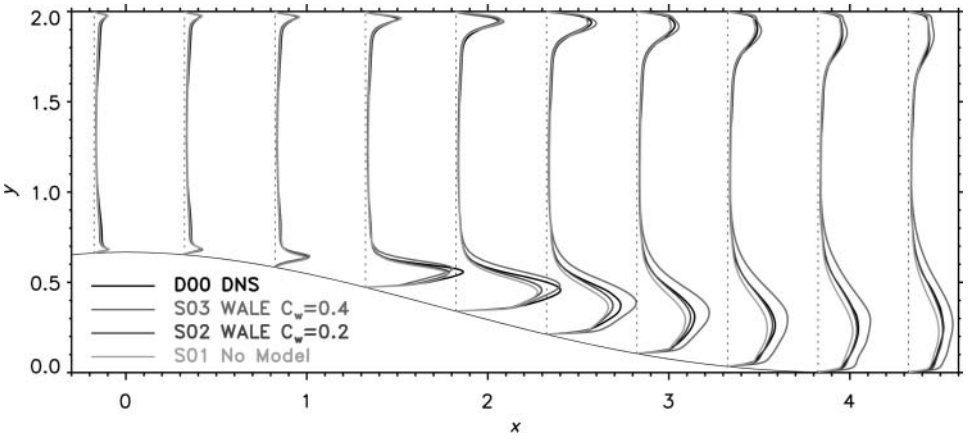

Figure 7. Kinetic energy distribution for the test case at $Re_\tau = 395$ using SAILOR code and the WALE subgrid-scale model on the fine mesh ($C_w = 0.0, 0.2, 0.4$).

simulation domain. This can be explained by the fact that the SGS energy transfer probably exhibits very different properties within the full domain, and especially in the region of minimum friction velocity. Marquillie et al. [19] have evidenced an intense generation of coherent structures in this region corresponding to a sharp peak of turbulent kinetic energy production. These small-scale coherent structures are probably due to sudden instabilities of low-speed streaks combined with inflectional mean velocity profiles. From an LES point of view, this phenomena must be associated with a strong backward energy transfer from the subgrid scales to the resolved scales (backscatter), which is not modeled by the standard turbulent viscosity SGS models.

To confirm the above observations, additional analysis of the turbulent kinetic energy distribution was performed. Figure 7 shows profiles of turbulent kinetic energy k compared with DNS for a fine mesh. The overall LES prediction of kinetic energy is very good. However, some discrepancies can be observed especially in the outer part of the boundary layer close to the curved wall. In the adverse pressure gradient region, enhancement of kinetic energy production is observed. One may observe that without the model and with $C_w = 0.4$, the turbulent kinetic energy level is not properly reflected. For the first case, the level is underpredicted while for the last case it is too high. By keeping the model constant equal to 0.2, perfect agreement is obtained in the entire computational domain. This consistency of results is important, because the length of the separation bubble is heavily dependent on the kinetic energy in the separated shear layer.

5.2. *Comparison of solvers: discretization method and implementation*

This section concerns the impact of the solver and discretization method in the streamwise direction. For this purpose, a comparison of C_f distributions without the model (see Figure 8a) as well as with the WALE model and $Cw = 0.4$ (see Figure 8b) have been analyzed. Most attention was paid to the region downstream from the top of the bump. In case of a coarse mesh, both LML and CUT solvers overpredict the skin friction coefficient on both walls. However, the LML solver gives considerably worse results, not only in the diverging, but also in the converging region. It does not predict the separation point at all. CUT results are significantly better and this seems to be the result of the higher order of

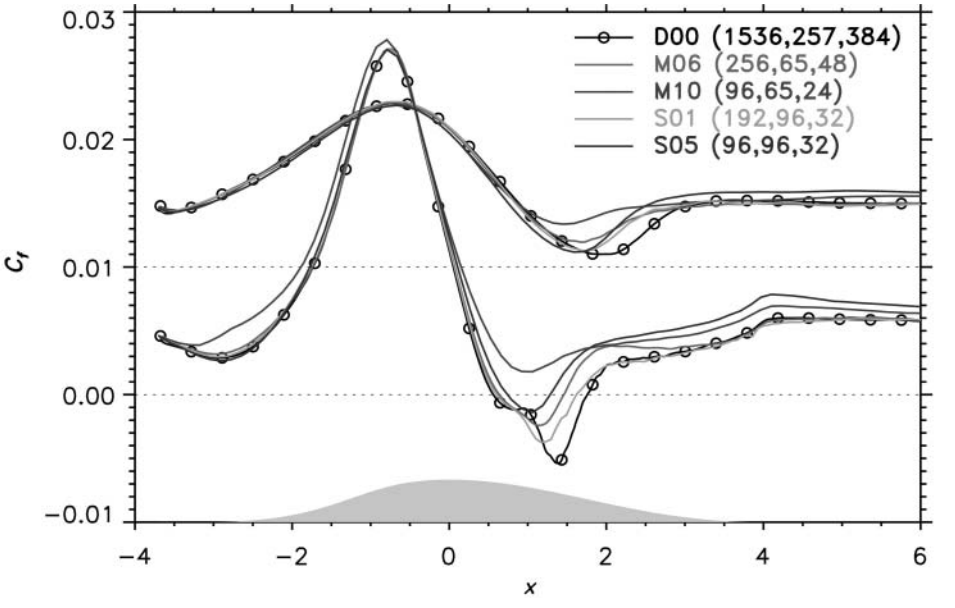

(a) C_f distributions, no subgrid scale model; CUT coarse and fine mesh; LML fine mesh and super fine mesh

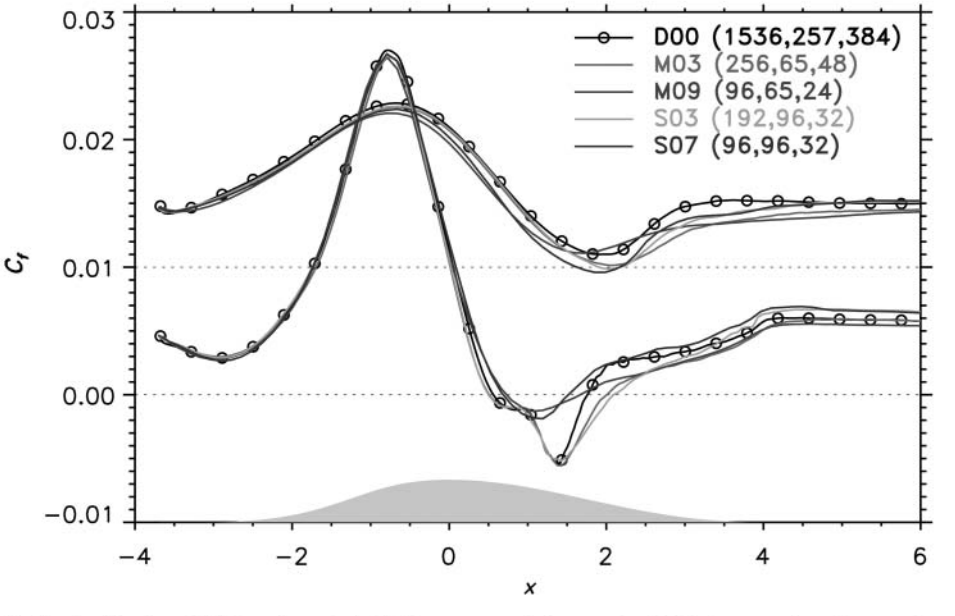

(b) C_f distributions WALE $C_w = 0.4$; CUT coarse and fine mesh; LML fine mesh and super fine mesh

Figure 8. C_f distribution with the two numerical codes for the test case at $Re_\tau = 395$ using the WALE subgrid-scale model with a 0.4 constant and the same test case with no subgrid-scale model.

discretization scheme applied in the streamwise direction (6th for CUT and 4th for LML). The same conclusion may be drawn based on the solution obtained for the refined mesh (in the streamwise direction) although for this case, the differences are less evident and are limited only to the region downstream of the separation point. However, one must keep in mind that the number of nodes in the streamwise direction for the LML simulations ($N_x = 256$) is higher by 33% than for the CUT simulation. Figure 8b shows a comparison of the skin friction distribution obtained for the model constant $C_w = 0.4$. In comparison to Figure 8a, the LML coarse case shows much better agreement with DNS than the case without the model does. However, with a coarse mesh, both CUT and LML solvers were not able to properly predict the minimum of C_f for the lower wall. The solutions obtained for fine meshes for both codes are very similar to each other. The influence of the high-order discretization is barely seen here, although one should keep in mind the 33% difference in the streamwise resolution of the mesh.

Summing up, one could conclude that it is clear that apart from the mesh refinement, discretization plays an important role in the final solution. It has been shown that to predict the separation point with a good accuracy the minimum resolution in streamwise direction is required and due to this fact the application of high-order discretization method seems to show some advantage. At the same time, it is clear that, for our test case and the investigated range of parameters, the effect of the model SGS viscosity is much more significant than the discretization level. As it was shown, these findings are valid at least for the given test case and to generalize these conclusions, further studies are necessary.

5.3. *Assessment of the role of subgrid scale model*

As stated above, the accuracy of the LES solution depends not only on the errors introduced by the discretization method, but also by the SGS model. This section is devoted to the analysis of the role of SGS models. The classical Smagorinsky and WALE models implemented in the SAILOR code and SISM, DSM, and WALE models implemented in the MFLOPS3D are investigated and compared over several grids.

In Figure 9, the skin friction distribution is presented for the WALE, Smagorinsky, and Dynamic Smagorinsky models. Analysis shows that the effect of the SGS model is not significant in the converging part of the channel. The influence of SGS closure is seen starting from the reattachment point. It is clear, as expected, that Smagorinsky shows the worst agreement with the DNS result. The Smagorinsky model (S04) did not predict either the minimum of the skin friction coefficient or the location of the reattachment point. Solutions obtained for the WALE model with two different solvers (S03 and M03) are very similar. When using a WALE model constant $C_w = 0.4$, which is assumed to be a reasonable choice in our case according to the previous analysis, neither results properly predict the exact location of the reattachment point, as discussed in Section 5.1, but reproduced the shape of C_f distribution with only a slight shift toward higher values. The differences between results obtained with the WALE and DSM models are also negligible and suggest that, for an appropriate mesh, both SGS models can be optimized for the simulation of near-wall flows subjected to an adverse pressure gradient with and without separation. The above results allow us to conclude that if the eddy viscosity is properly scaled near the wall (DSM and WALE models), the influence of the SGS model is of lesser importance than the effect of mesh resolution. The above conclusions were confirmed by conducting a simulation for the $Re_\tau = 617$ case with the MFLOPS3D (see Figure 10). This case is then

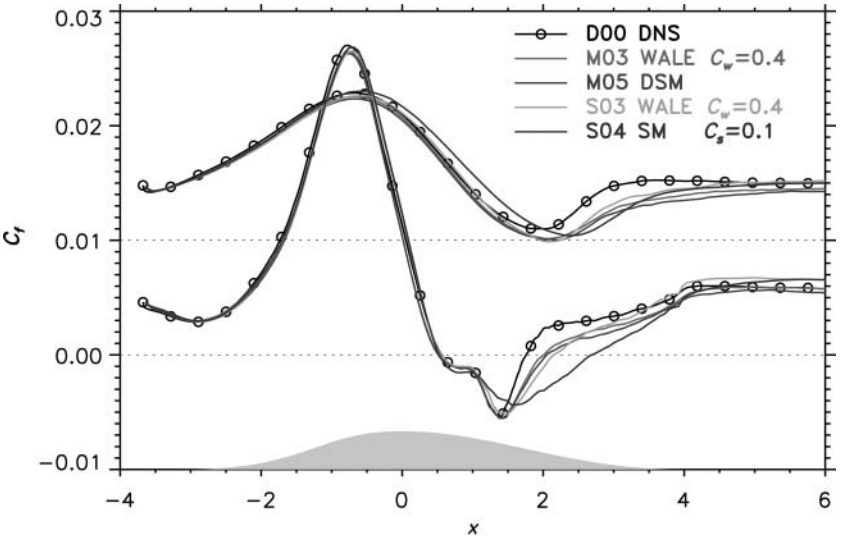

Figure 9. C_f distributions with SAILOR code on fine mesh using the Smagorinsky model and the WALE subgrid-scale model and with MFLOPS3D code with superfine mesh using the dynamic Smagorinsky model and the WALE model.

investigated using the SISM model. For this last model, up to six constants ranging from 0.08 to 0.18 were tested for the grid ($288 \times 97 \times 72$).

The best result was obtained for a constant of 0.09, not far from the classical value of the standard Smagorinsky model for channel flows. It is easy to see the positive effect of each of the SGS models and the relatively small difference between consecutive results. Here again, at a fine-enough resolution, the DSM and WALE models produce very similar results both at the lower wall and at the upper wall. The SISM model slightly underpredicts

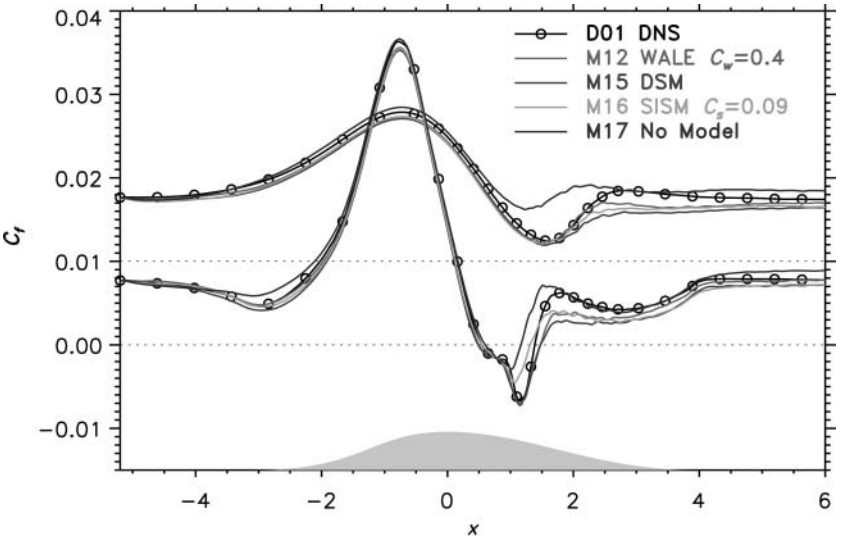

Figure 10. C_f distribution: influence of the subgrid-scale model ($Re_\tau = 617$).

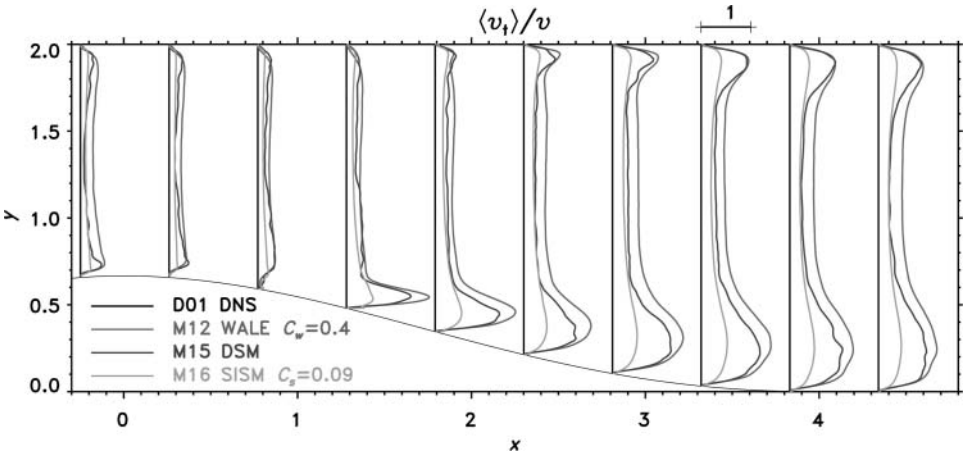

Figure 11. Turbulent viscosity profiles for the DSM, WALE, and SISM models ($Re_\tau = 617$).

the separation region at the lower wall. Despite similar results on the mean flow, the three tested models produce different average values of turbulent viscosity (see Figure 11) even between the DSM and WALE models. However, while the spatial distribution of the SGS dissipation is quite different for the two models, both produce correct results for the mean flow. The resolved turbulent kinetic energy is compared in Figure 12 with the total turbulent kinetic energy of the DNS and the resolved turbulent kinetic energy from the filtered DNS. The two SGS models lead to resolved turbulent kinetic energy peaks which are larger than the filtered DNS and even larger than the total turbulent kinetic energy peaks in the downstream part of the APG. However, the intensity of these peaks is extremely sensitive to the mean velocity profile at the beginning of the APG region. As the mean friction velocity is not precisely modeled, conclusions on the resolved turbulent energy are not easy to draw.

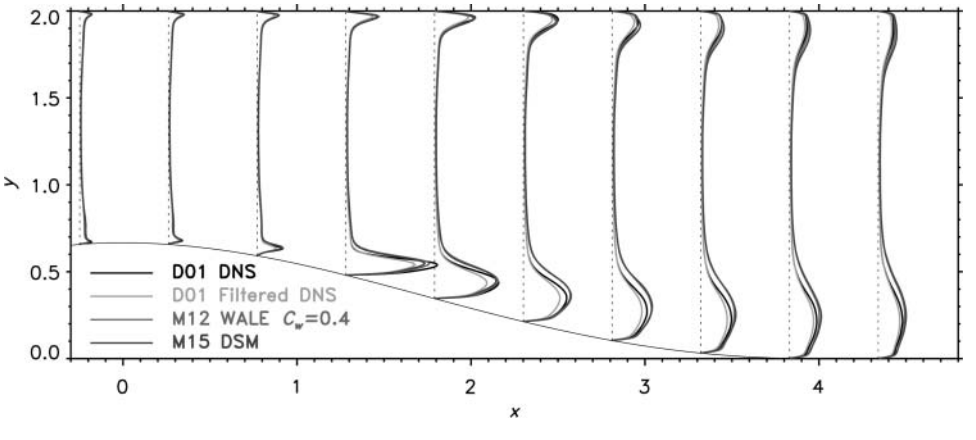

Figure 12. Resolved turbulent kinetic energy profiles for the DSM and WALE models ($Re_\tau = 617$).

6. Conclusions

The paper presents the results of the application of LES to turbulent channel flow with a varying pressure gradient obtained by the adequate curvature of one of the walls. Due to a reversal of the flow where the turbulence transport is dictated by the dynamics of the large-scale eddies, such a case is well suited to demonstrate the predictive features of the LES technique. The main objective of the paper was to assess various SGS models implemented in two different codes as well as the sensitivity of the predictive accuracy to grid resolution. It was demonstrated that all SGS models require a comparable minimum grid refinement in order to capture accurately the recirculation region. Notably, it has been shown that the grid refinement in the streamwise direction is the leading parameter when considering the accuracy of the results, whereas increasing the resolution in the spanwise and normal directions does not lead to significantly better results in the separation region but may affect the solution at the flat upper wall. Common analysis of the grid resolution and the SGS model constant values shows a strong interrelation between the two. It has been demonstrated that, for the two high-order codes used in the present study, the role of the SGS viscosity is significant for any of the tested discretizations. On the other hand, when the eddy viscosity is properly scaled near the wall (DSM and WALE models), the influence of the SGS model is rather small when the model constant is optimized. One could also conclude that, in the case of LES with implicit filtering, the grid spacing must be associated with the discretization method.

The present study has suggested the benefit of higher order discretization method in streamwise direction as a minimum resolution is required in this direction to predict the separation point with a good accuracy. These findings are valid for the given test case, so to generalize them further studies are necessary.

The present study also confirmed that, for this nontrivial test case, the model constants are not universal and need to be calibrated for each LES configuration. In the presented configuration of APG flows, which lead to a sudden turbulent kinetic energy peak associated with small-scale coherent structures, one could expect better performance from SGS models which allow for backward energy transfer from subgrid scales to resolved scales.

Acknowledgements

This work was supported by CISIT (International Campus on Safety and Inter-modality in Transport) and WALLTURB (A European synergy for the assessment of wall turbulence), which is funded by the EC under the 6th framework program (CONTRACT: AST4-CT-2005-516008). The DNS was performed through two successive DEISA Extreme Computing Initiatives (DEISA is Distributed European Infrastructure for Supercomputing Applications). This work was granted access to the HPC resources of IDRIS (Institut du Developpement et des Ressources en Informatique Scientifique) under the allocation 2010-021741 made by GENCI (Grand Equipement National de Calcul Intensif) and to the HPC resources of Lille University.

References

[1] J. Meyers, B.J. Geurts, and M. Baelmans, *Database analysis of errors in large-eddy simulation*, Phys. Fluid. 15 (2003), pp. 2740–2755.

[2] J. Meyers, P. Sagaut, and B. Geurts, *A computational error assessment of central finite-volume discretizations in large-eddy simulation using a Smagorinsky model*, J. Comput. Phys. 227 (2007), pp. 156–173.

[3] U. Piomelli and E. Balaras, *Wall-layer models for large-eddy simulations*, Ann. Rev. Fluid Mech. 34 (2002), pp. 349–374.

[4] J. Meyers, *Error-landscape assessment of large-eddy simulations: a review of the methodology*, J. Sci. Comput. 49 (2011), pp. 65–77.
[5] J. Fröhlich, J.A. Denev, C. Hinterberger, and H. Bockhorn, *On the impact of tangential grid refinement on subgrid-scale modelling in large eddy simulation*, in *Numerical Methods and Applications: 6th International Conference*, NMA 2006, T. Boyanov, S. Dimova, G. Nikolov, and K. Georgiev, eds., Springer, Hiedelberg, 2006, pp. 550–557.
[6] J. Meyers and P. Sagaut, *Is plane channel flow a friendly test-case for the testing of LES subgrid scale models ?*, Phys. Fluid. 19 (2007), p. 048105.
[7] J. Fröhlich, C.P. Mennen, W. Rodi, L. Temmerman, and A. Leschziner, *Highly resolved large-eddy simulation of separated flow in a channel with streamwise periodic constrictions*, J. Fluid. Mech. 526 (2005), pp. 19–66.
[8] M. Hahn and D. Drikakis, *Assessment of large-eddy simulation of internal separated flow*, J. Fluids Eng. 131 (2009), pp. 071201–071215.
[9] M. Breuer, N. Peller, C. Rapp, and M. Manhart, *Flow over periodic hills – numerical and experimental study in a wide range of Reynolds numbers*, Comput. Fluid. 38 (2009), pp. 433–457.
[10] J.-P. Laval, W. Elsner, L. Kuban, and M. Marquillie, *LES modeling of converging diverging turbulent channel flow*, in *Progress in Wall Turbulence: Understanding and Modelling* (ERCOFTAC Series), M. Stanislas, J. Jimenez, and I. Marusic, eds., Springer, New York, 2009, pp. 355–363.
[11] M. Marquillie, J.-P. Laval, and R. Dolganov, *Direct numerical simulation of separated channel flows with a smooth profile*, J. Turbul. 9 (2008), pp. 1–23.
[12] E. Leveque, F. Toschi, L. Shao, and J.-P. Bertoglio, *Shear-improved Smagorinsky model for large-eddy simulation of wall-bounded flows*, J. Fluid Mech. 570 (2007), pp. 491–502.
[13] F. Nicoud and F. Ducros, *Subgrid-scale stress modelling based on the square of the velocity gradient tensor*, Flow. Turbul. Combust. 62 (1999), pp. 183–200.
[14] C.A.J. Fletcher, *Computational Techniques for Fluid Dynamics*, Springer-Verlag, Hiedelberg, 1991.
[15] S.K. Lele, *Compact finite difference schemes with spectral-like resolution*, J. Comp. Phys. 103 (1992), pp. 16–42.
[16] R. Pasquetti, R. Bwemba, and L. Cousin, *A pseudo-penalization method for high Reynolds number unsteady flows*, Appl. Numer. Math. 58 (2008), pp. 946–954.
[17] D.K. Lilly, *A proposed modification of the germano subgrid-scale closure method*, Phys. Fluids A 4 (1992), pp. 633–635.
[18] J.-P. Laval and M. Marquillie, *Direct numerical simulations of converging-diverging channel flow*, in *Progress in Wall Turbulence: Understanding and Modelling* (ERCOFTAC Series), M. Stanislas, J. Jimenez, and I. Marusic, eds., Springer, New York, 2009, pp. 203–210.
[19] M. Marquillie, U. Ehrenstein, and J.-P. Laval, *Instability of streaks in wall turbulence with adverse pressure gradient*, J. Fluid Mech. 681 (2011), pp. 205–240.